PNAS RESEARCH ARTICLE | BIOCHEMISTRY

Discovery of highly potent and ALK2/ALK1 selective kinase inhibitors using DNA-encoded chemistry technology

Ravikumar Jimmidi[a,b,1], Diana Monsivais[a,b,1], Hai Minh Ta[a,b,1], Kiran L. Sharma[a,b], Kurt M. Bohren[a,b], Srinivas Chamakuri[a,b], Zian Liao[a,b,c], Feng Li[a,b,d], John M. Hakenjos[a,b], Jian-Yuan Li[a,b], Yuji Mishina[e], Haichun Pan[e], Xuan Qin[a,b], Matthew B. Robers[f], Banumathi Sankaran[g], Zhi Tan[a,b,h], Suni Tang[a,b], Yasmin M. Vasquez[a,b], Jennifer Wilkinson[f], Damian W. Young[a,b,h], Stephen S. Palmer[a,b], Kevin R. MacKenzie[a,b,h], Choel Kim[a,b,h], and Martin M. Matzuk[a,b,c,d,h,2]

Affiliations are included on p. 10.

Contributed by Martin M. Matzuk; received July 1, 2024; accepted October 5, 2024; reviewed by Jeffrey G. Martin and Thomas B. Thompson

Activin receptor type 1 (ACVR1; ALK2) and activin receptor like type 1 (ACVRL1; ALK1) are transforming growth factor beta family receptors that integrate extracellular signals of bone morphogenic proteins (BMPs) and activins into Mothers Against Decapentaplegic homolog 1/5 (SMAD1/SMAD5) signaling complexes. Several activating mutations in ALK2 are implicated in fibrodysplasia ossificans progressiva (FOP), diffuse intrinsic pontine gliomas, and ependymomas. The ALK2 R206H mutation is also present in a subset of endometrial tumors, melanomas, non–small lung cancers, and colorectal cancers, and ALK2 expression is elevated in pancreatic cancer. Using DNA-encoded chemistry technology, we screened 3.94 billion unique compounds from our diverse DNA-encoded chemical libraries (DECLs) against the kinase domain of ALK2. Off-DNA synthesis of DECL hits and biochemical validation revealed nanomolar potent ALK2 inhibitors. Further structure–activity relationship studies yielded center for drug discovery (CDD)-2789, a potent [NanoBRET (NB) cell IC_{50}: 0.54 μM] and metabolically stable analog with good pharmacological profile. Crystal structures of ALK2 bound with CDD-2281, CDD-2282, or CDD-2789 show that these inhibitors bind the active site through Van der Waals interactions and solvent-mediated hydrogen bonds. CDD-2789 exhibits high selectivity toward ALK2/ALK1 in KINOMEscan analysis and NB K192 assay. In cell-based studies, ALK2 inhibitors effectively attenuated activin A and BMP-induced Phosphorylated SMAD1/5 activation in fibroblasts from individuals with FOP in a dose-dependent manner. Thus, CDD-2789 is a valuable tool compound for further investigation of the biological functions of ALK2 and ALK1 and the therapeutic potential of specific inhibition of ALK2.

DEL | kinase inhibitors | X-ray Crystallography

Significance

Identifying potent and specific small molecule inhibitors of Activin receptor type 1 (ALK2), one of the bone morphogenic proteins (BMP) and activin type 1 receptors, has been an ongoing challenge hindering the development of effective therapeutics for fatal diseases such as fibrodysplasia ossificans progressiva (FOP), diffuse intrinsic pontine gliomas (DIPGs), and ependymomas. Our study describes the identification and subsequent optimization of CDD-2789, a nontoxic and potent inhibitor of ALK2 that displays high kinase selectivity, metabolic stability, and activity in an FOP cell model. CDD-2789 was identified using DNA-encoded chemistry technology (DEC-Tec) by screening a library of 3.94 billion unique compounds, thereby demonstrating the utility of this platform for developing potentially life-saving therapeutics.

Bone morphogenetic proteins (BMPs) and activins are conserved, secreted ligands belonging to the transforming growth factor beta (TGFβ) family that orchestrate crucial functions in development, cell proliferation, differentiation, and apoptosis (1). Initially recognized for their capacity to induce ectopic bone formation, BMPs now stand acknowledged for regulating diverse cellular processes encompassing various tissue types, such as kidney, skeletal muscle, heart, and reproductive organs (1, 2). Additionally, BMPs and activins and their corresponding receptors assume pivotal roles in numerous pathophysiological contexts, thereby emerging as compelling targets for therapeutic intervention.

BMPs and activins are produced as inactive pre-propeptides, featuring N-terminal signal peptides and C-terminal mature domains, which are processed enzymatically to obtain their active forms (3–5). BMPs signal by binding to receptor complexes composed of type 1 [activin receptor like type 1 (ALK1) ALK1/ALK2/ALK3/ALK6] and type 2 [ACVR2A/ACVR2B/bone morphogenetic protein receptor type 2 (BMPR2)] receptors that are located on the cell surface. BMP receptors are single-pass transmembrane proteins, featuring an extracellular ligand-binding domain alongside a cytoplasmic kinase domain (KD). When a ligand binds, the BMP type 2 receptor catalyzes phosphorylation of the glycine serine (GS) domain within the BMP type 1 receptor, instigating a structural alteration in the type 1 receptor conducive to adenosine triphosphate (ATP) binding. After ligand-bound activation of the receptors, SMAD1, SMAD5, and SMAD8 transcription factors are phosphorylated and activated (6, 7).

Mutations within the ALK2 receptor induce a change in the ligand specificity of ALK2 and enable stimulation of SMAD1/5 by a broader group of TGFβ family proteins including activin A. Patients with fibrodysplasia ossificans progressiva (FOP) develop heterotopic ossification (HO) in various soft tissues, including muscles, ligaments, and tendons

Reviewers: J.G.M., Biogen; and T.B.T., University of Cincinnati.

Competing interest statement: A provisional patent was submitted by R.J., D.M., K.M.B., F.L., J.-Y.L., Z.T. D.W.Y., S.S.P., and M.M.M. from Baylor College of Medicine.

[1]R.J., D.M., and H.M.T. contributed equally to this work.

[2]To whom correspondence may be addressed. Email: mmatzuk@bcm.edu.

This article contains supporting information online at https://www.pnas.org/lookup/suppl/doi:10.1073/pnas.2413108121/-/DCSupplemental.

Published November 14, 2024.

(8, 9). Patients with FOP have a defective BMP signaling pathway that is characterized by an activating mutation in ALK2 (R206H). Diffuse intrinsic pontine gliomas (DIPGs) are aggressive pediatric brain tumors that arise in the brainstem at approximately age 6 to 7, are universally fatal and have a mean overall survival of 9 to 12 mo (10). These aggressive tumors are characterized by somatic heterozygous mutations in ALK2, which are observed in ~24% of patients (11, 12). The mutations that are most frequently observed include those occurring in the GS domain (R206H) and in the KD (G328E and G328V), and cause ligand-induced activation of SMAD1/5/8 (12). Due to its critical role in the regulation of iron metabolism, targeting ALK2 may also offer therapeutic potential in addressing conditions such as atherosclerosis, severe iron deficiency anemia, and various forms of anemia, including the inflammatory-driven anemia of chronic disease. Thus, inhibition of the kinase activity of ALK2 is a promising approach for the treatment of FOP (13), DIPGs (9), ependymomas, endometrial cancer (14), atherosclerosis (15), iron deficiency anemia (16), tumor vasculogenesis (17, 18), and Sjögren's syndrome (19).

Given the therapeutic potential of ALK2, many research groups from academia and pharmaceutical companies are investigating ALK2 and inhibitors in the context of various disease models (20–22). To date, several potent ALK2 inhibitors have been identified using traditional high-throughput screening and structure-guided approaches (23–27). Despite their potency, the majority of these inhibitors exhibit poor selectivity among TGFβ family receptors (20). Dorsomorphin was the first inhibitor identified through high-throughput screens using ventralization assays in zebrafish models (23). Structure-based optimization yielded LDN-193189, which demonstrated increased pharmacokinetic stability relative to dorsomorphin (28). LDN-212854 was developed as an ALK2-biased inhibitor with the potential to inhibit HO in an FOP mouse model, but similar to other compounds, lacked specificity over the other type 1 receptors (24). Recently, Davis et al. created a new dorsomorphin analog, BLU-782, that prevented cartilage and HO in a mouse model, although it still bound multiple off-target kinases, as well as ALK1, ALK2, and ALK6 (27). Thus, to avoid potential off-target toxicity of nonspecific inhibitors, there is a need to develop potent, specific, and stable ALK2 inhibitors.

DNA-encoded chemistry technology (DEC-Tec) is a cost-effective and rapidly emerging platform for identifying drug-like molecules with high binding affinity to target proteins (25, 26, 29, 30). DNA-encoded chemical libraries (DECLs) of drug-like compounds are covalently attached to DNA with a unique DNA barcode that corresponds to each library molecule, thereby allowing for precise identification of each molecule in a pool of billions of different compounds. During library construction, sequential cycles of covalent attachment of chemical building blocks to a molecular scaffold on DNA is followed by ligation of a corresponding DNA barcode (31). DECLs are screened as multibillion compound mixtures against a His-tagged protein target. DNA-encoded molecules with affinity to the His-tagged protein are separated from the mixture using nickel-magnetic beads that bind the tag. Next-generation sequencing and informatic analysis allow determination of the bound DNA barcode sequences, and, thus, the structures of the enriched drug-like compounds are identified. Because DECLs are composed of billions of compounds, they are capable of rendering potent small molecule hits toward a wide category of biological targets.

Using our DECL collection (multibillion unique molecules), which includes both structurally diverse as well as biased libraries (kinases, proteases, and lactamases), we have identified small molecule leads for several disease-relevant protein targets including serine/threonine kinase 33 (32), BMPR2 (2), pan-ephrin receptor kinases (33), BET family bromodomain 1 (34) and bromodomain 2 (35), thrombin (36), and infectious disease targets SARS-CoV2 main protease [M^{pro}; both covalent (37) and noncovalent inhibitors (38)] and β-lactamases (39).

In this study, we used DEC-Tec to identify potent inhibitors targeting the KD of ALK2. We screened our DECL collection of billions of molecules against the ALK2 KD, resulting in significant enrichment of hits. Following a thorough analysis of the selection profile, promising hits were synthesized without DNA tags. Subsequent biochemical and cellular assays confirmed the activity of these hits. Further exploration through structure–activity relationsbone morphogenic proteinhip (SAR) studies led to the development of more stable and highly selective ALK2 inhibitors. The X-ray crystal structures of these inhibitors bound to the ALK2 KD were obtained, validating their close interaction with the KD pocket. Both the original DECL hit compounds and their analogs exhibited excellent ALK2 inhibition and demonstrated significant cellular activity. Furthermore, our newly identified ALK2 inhibitors effectively suppressed BMP2, BMP6, and BMP7-induced luciferase transactivation in a BMP reporter system and decreased Phosphorylated SMAD1/5 (pSMAD1/5) activation in fibroblasts from both FOP and wild-type (WT) individuals in a dose-dependent manner.

Results and Discussion

DEC-Tec Affinity Selection with ALK2 Protein and Evaluation of Hit Compounds. To identify putative ALK2 hits, we screened a pool of 45 distinct chemical libraries, collectively comprising 3.94 billion compounds, with our DEC-Tec platform using a His-tagged ALK2 KD produced by baculovirus in SF21 insect cells. For affinity selections, the DECL pool was incubated with 0.06 μM His-tagged ALK2 kinase, pulled down with nickel-NTA magnetic beads, washed, and eluted by heating. Three rounds of selection were performed, with parallel experiments that did not include ALK2 protein (no-target control, NTC) or that included both ALK2 and the competitive inhibitor, LDN-193189. PCR-amplified samples from NTC, ALK2, and ALK2 plus LDN-193189 kinase inhibitor experiments were subjected to Illumina next-generation sequencing. Utilizing our informatics pipeline (31), we decoded the chemical structures bound to ALK2 by analyzing the encoded DNA sequences and assessed compound enrichment through statistical analysis.

Fig. 1 illustrates the enrichment of DECL selections of ALK2, displaying normalized z-scores (22) and counts for enriched hits from qDOS18_2 library, which is based on a benzimidazole core scaffold. These hits do not show enrichment in the selection group with LDN-193189 added, suggesting that these compounds likely bind to the ATP-binding pocket (*SI Appendix*, Fig. S1). Within this library, various tri-synthons (union of three BBs) are enriched, with counts ranging from 38 to 3. Among these tri-synthons, we observed close structure enrichment relationships (SER) with building blocks BB1 (blue), BB2 (red), and BB3 (black). From these binders, we initially synthesized CDD-2622 (*R,R*-isomer), CDD-2206 (*S,S*-isomer), along with CDD-2205. CDD-2622 and its analogs were synthesized within 3 to 4 steps (Scheme 1) from commercially available BBs. The synthetic route was started with 3-fluoro-4-nitrobenzoic acid (4), which was subjected to an amidation reaction with amine **5** to yield amide intermediate **6**. Next, an S_NAr reaction was performed with primary amine **7** to yield the penultimate compound **8**. Finally, the benzimidazole CDD-2622 was obtained from a one-pot dithionate-mediated reduction of the nitro group followed by condensation with 3,4,5-trimethoxy benzaldehyde (38).

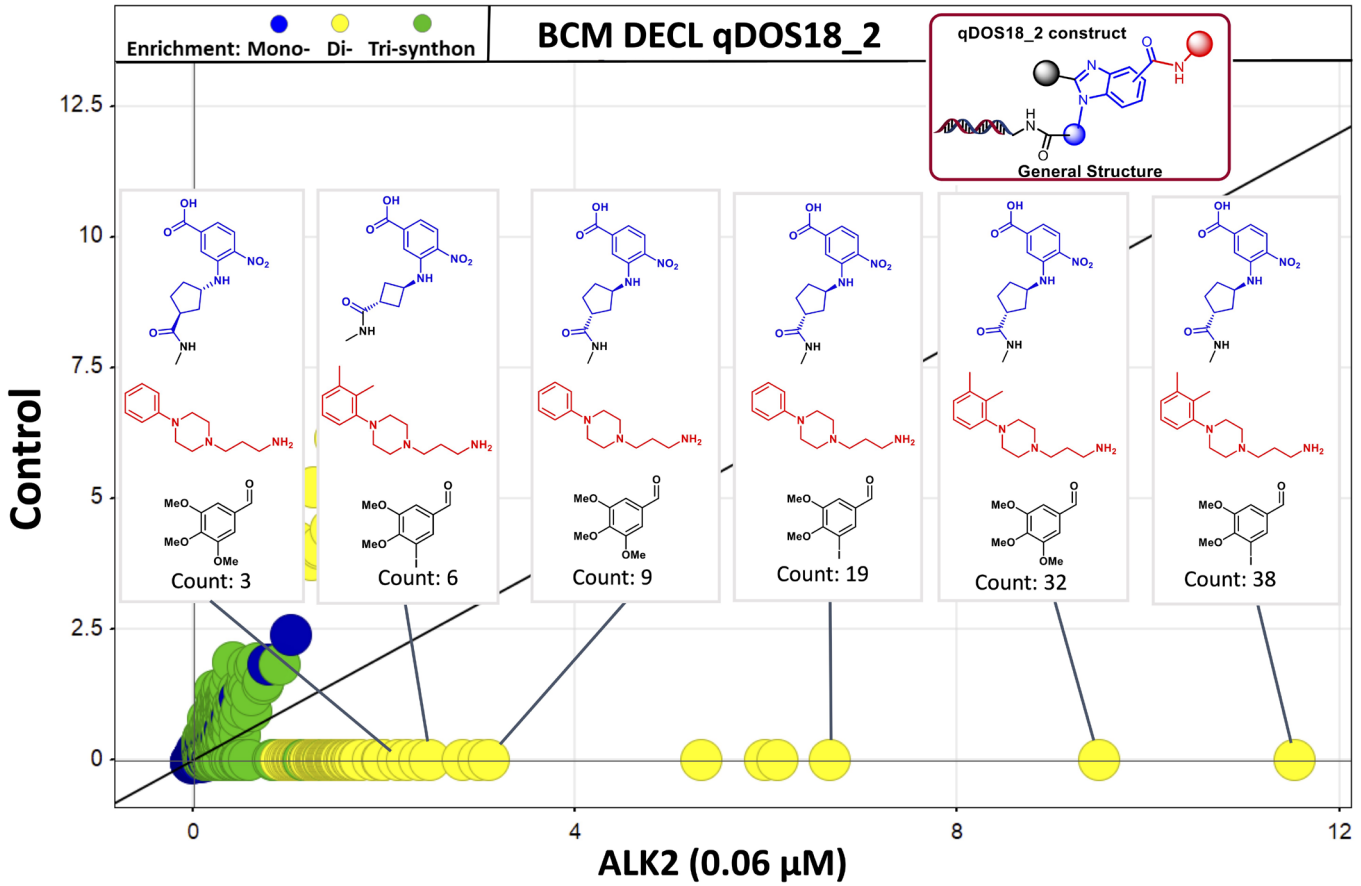

Fig. 1. Enrichment profile of ALK2 binders using Baylor College of Medicine DECLs. Enrichment profile of ALK2 at 0.06 µM from qDOS18_2. The selection data show the enrichment of the similar BB1 (blue) BB2 (red), and BB3 (black). Hits from a DNA-encoded library ALK2 selection plotted at their enrichment z-scores for ALK2 (*x*-axis versus z-score for the selection against NTC on the *y*-axis.

To assess the ability of the ALK2 binders for inhibition of in vitro kinase activity, a kinase LanthaScreen binding assay was performed using the Thermo Fisher Scientific's SelectScreen™ Profiling Service. Our selection hits CDD-2622, CDD-2206, and CDD-2205 showed equivalently high potency toward ALK2, with K_d values of 1.3 nM, 1.4 nM, and 0.9 nM, respectively (Fig. 2 and *SI Appendix*, Fig. S2*B* and Table S1). These results corroborated our selection results given that the enriched compounds directly from DECL showed inhibition of ALK2 with low nanomolar activity. Next, we synthesized CDD-2235 by substituting

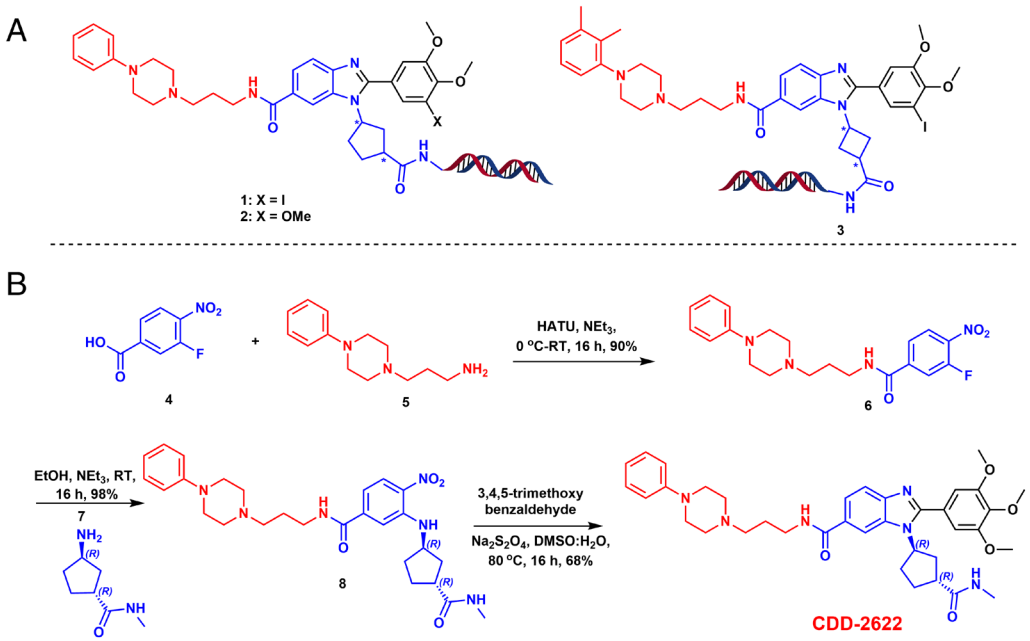

Scheme 1. DNA-encoded chemical library selections of ALK2. (*A*) Hit compounds enriched from selections. (*B*) Off-DNA synthesis of CDD-2622.

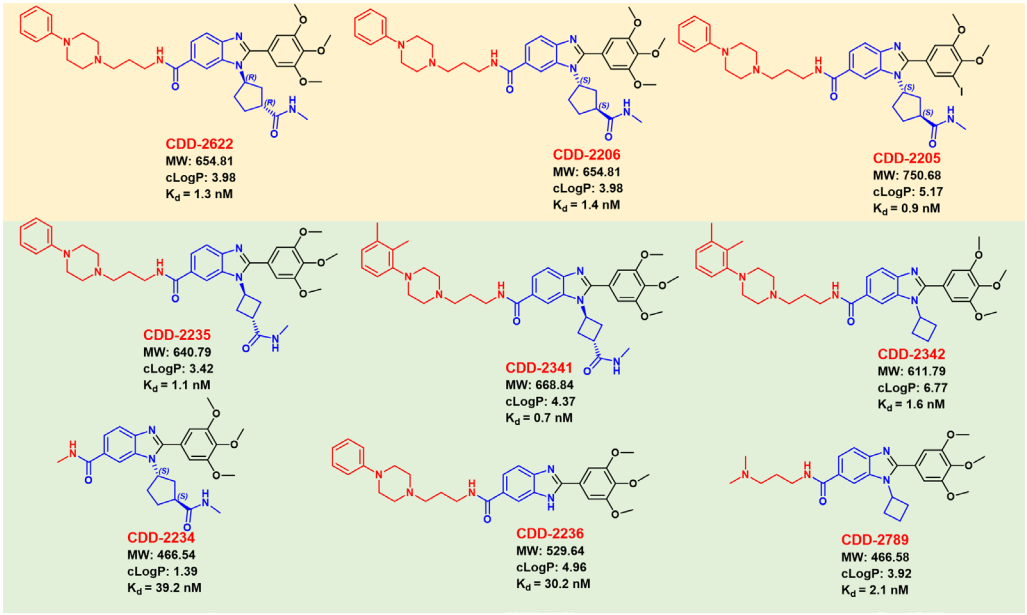

Fig. 2. ALK2 hits, analogs synthesized off-DNA. Numbers indicate K_d values determined as described in *Materials and Methods*. Yellow background ALK2 inhibitors directly from DEL library and green background inhibitors that are analogs synthesized based on DEL hits.

the cyclopentyl ring with cyclobutyl ring and CDD-2341 by introducing methyl substituted phenyl ring. As anticipated, both CDD-2235 (K_d = 1.1 nM) and CDD-2341 (K_d = 0.7 nM) exhibited excellent potency to ALK2. To assess the SAR near the former DNA attachment point (methylamide on cyclobutyl ring) in CDD-2341 and CDD-2235, we trimmed the methylamide to yield CDD-2342 (K_d = 1.6 nM), and CDD-2315 (K_d = 0.8 nM), both maintained similar potency as parent compounds. However, further truncation of the cyclobutyl group resulted in a 30-fold decrease in potency (CDD-2236, K_d = 30.2 nM). Furthermore, synthesis of CDD-2316, featuring a linear N-methyl-butylamide, led to a more than 50-fold reduction in activity (K_d = 51.4 nM). These findings collectively suggest that the cyclobutyl ring is important for ALK2 inhibition.

Kinase Selectivity Profile of CDD-2342. To ascertain the kinase selectivity of CDD-2342, we conducted a KINOMEscan assay against 403 kinases at 1 μM concentration. As illustrated in Fig. 3*A*, CDD-2342 exhibits significant selectivity for ALK1 and ALK2 over other kinases (Table 1). To validate these findings, LanthaScreen binding assays of ALK1, as well as other type 1 and type 2 TGFβ family kinases were performed. As indicated in Table 1, CDD-2342 is twofold selective toward ALK2 (K_d = 1.6 nM) over ALK1 (K_d = 3.2 nM) and highly selective with respect to TGFβ receptors, and LCK, and SLK kinases. However, while CDD-2342 is very potent, its metabolic stability in human liver microsomes (HLM) and mouse liver microsomes (MLM) (Table 2 and *SI Appendix*, Fig. S3) is too low to calculate the half-life. We identified and synthesized two major metabolites of CDD-2342; however, both metabolites CDD-2464 (K_d = 79.0 nM) and CDD-2465 (K_d = 15.4 nM) (*SI Appendix*, Fig. S3); showed reduced potency. Further, we focused on SAR studies to optimize the metabolic stability and drug-like properties of CDD-2342.

Exploration of SAR to Optimize the Selectivity, Activity, Solubility, and Metabolic Stability of ALK2 Inhibitors. Having established key features for binding from the DEL, we next focused on synthesizing compounds with more optimal properties. We initiated our SAR studies by interrogating compounds with different R^1 substitutions (*SI Appendix*, Table S1). Truncating the phenyl-piperazine containing propyl to methyl (CDD-2234) and eliminating the propyl linker (CDD-2279) markedly diminished the activity, underscoring the significance of the linker. Substituting the N-phenyl group of piperazine with an N-methyl group (CDD-2280) led to a 10-fold reduction in activity, while further truncation of the piperazine ring and substitution with N,N-dimethylpropyl group in CDD-2281 resulted in K_d of 5.2 nM. Substitution of the R^1 group with a methylpiperidine group (CDD-2282) exhibited good inhibition (K_d = 5.9 nM).

Next, we proceeded to investigate the impact of substitutions at the R^3 position of the benzimidazole scaffold. To assess the influence of methoxy groups on the phenyl ring, we synthesized 3,5-dimethoxy (CDD-2314, K_d = 6.9 nM), mono-methoxy (CDD-2313, K_d = 5.6 nM), de-methoxy (CDD-2317, K_d = 57.4 nM), 4-carboxamide (CDD-2339, K_d = 34.1 nM), and 3-fluoro-5-methoxy (CDD-2340, K_d = 6.9 nM) analogs, which all led to a decrease in activity. The 2,5-dimethoxy (CDD-2420, K_d = 0.9 nM) and 3,4-dimethoxy (CDD-2421, K_d = 2.1 nM) analogs displayed similar potency compared to the parent compound CDD-2341 (K_d = 0.7 nM). These findings underscore the collective contributions of all three methoxy groups at the R^3 position as important.

Among the analogs synthesized, CDD-2281 displayed excellent solubility (199.6 μM, Table 2) and high metabolic stability in MLM ($t_{1/2}$ = 13.4 h) and HLM ($t_{1/2}$ = 12.8 h) To determine whether further potency was attainable, we explored different R^3 groups that varied substitutions on the phenyl ring, but these modifications did not increase potency (as detailed in *SI Appendix*, Fig. S2 *A* and *C*). However, truncation of the amide group on the cyclobutyl moiety led to CDD-2789, having a lower molecular weight (466.58 Da), high potency (K_d = 2.1 nM), excellent metabolic stability, and high solubility (200 μM). To assess the kinase specificity of CDD-2789, we conducted a KINOMEscan assay at 1 μM concentration. As depicted in Fig. 3*B*, CDD-2789 exhibited remarkable selectivity for ALK2 and ALK1 compared to other kinases, similar to CDD-2342. These findings were further validated through LanthaScreen binding assays performed against ALK2/ALK1 and other type 1 and type 2 TGFβ family receptors,

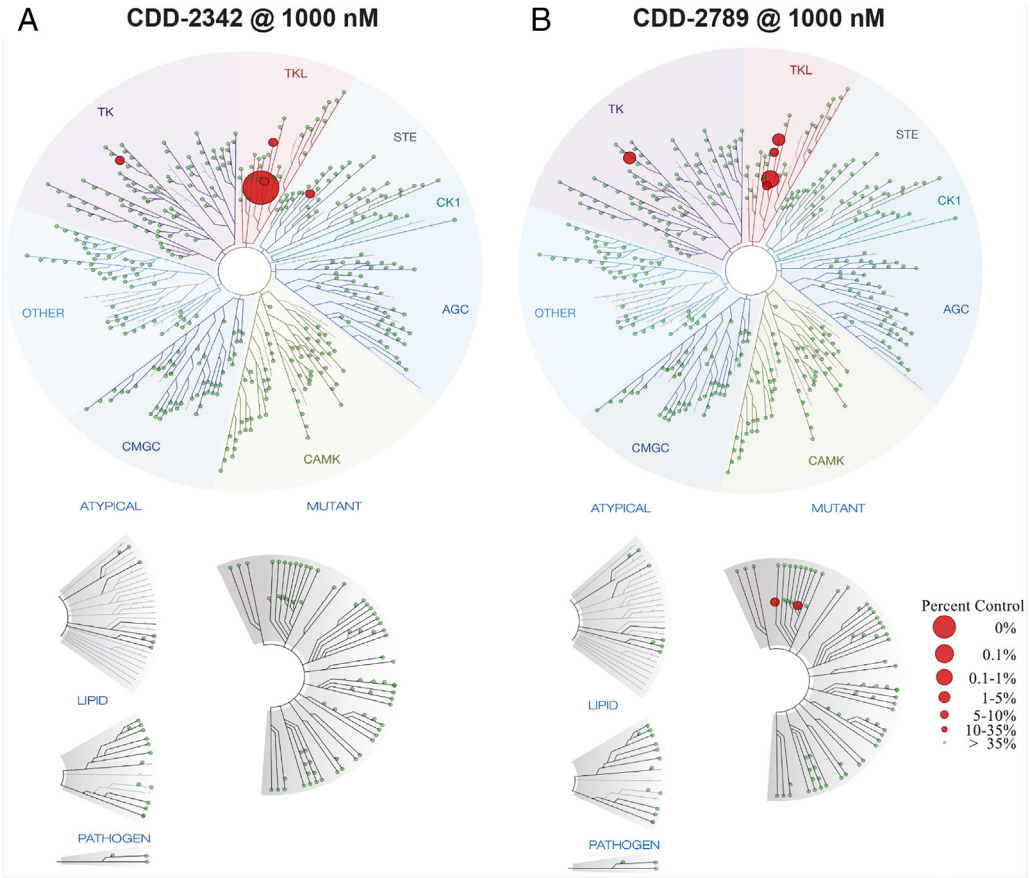

Fig. 3. Kinase selectivity profile of compounds CDD-2342, and CDD-2789. Compounds were assayed at 1 μM against 403 kinases using the DiscoveRx KINOMEscan screen. Compound selectivity is represented in a TREEspot kinase dendrogram view of the human kinome phylogenetic tree. (*A*) 12% percent control for CDD-2342, and (*B*) 1.2% percent control for CDD-2789, % inhibition = 1−%control; the, lower the percent control and the larger the red circles indicate stronger inhibition against the corresponding kinases; all other kinases tested were inactive as indicated by the green circles.

indicating that CDD-2789 is highly selective for ALK2/ALK1 compared with other TGFβ kinases (Table 1). Furthermore, CDD-2789 is nontoxic to HepG2 cells at 100 μM (*SI Appendix*, Fig. S4). Pharmacokinetic studies of CDD-2789 in mice indicate that CDD-2789 has a 3.42 h plasma $t_{1/2}$ (*SI Appendix*, Fig. S5).

Crystal Structures of ALK2 with CDD-2281, CDD-2282, or CDD-2789. To understand the binding mode and the SAR, crystal structures of ALK2 KD bound to CDD-2281, CDD-2282, and CDD-2789 were determined (Fig. 4*A* and *SI Appendix*, Table S3 for data collection and refinement statistics) [Protein Data Bank (PDB) ID: 9D8F, 9D8Z, 9D8E]. All of the ALK2:inhibitor complexes crystallized in the same space group with nearly identical unit cell dimensions. The asymmetric unit of ALK2:inhibitor complex crystals contain two ALK2 monomers with clear density for bound CDD compounds (Fig. 4*B*). The two monomers within each complex are nearly identical (rmsd > 1 Å for Cα atoms for all three structures) and show the same binding mode with minor differences in their contacts. The benzimidazole and its cyclobutane and tri-O-methyl phenyl substituents superimpose well across all three structures. The inhibitors bind the kinase active site through van der Waals contacts and several water-mediated hydrogen bonds, but without forming any direct hydrogen bonds.

CDD-2789 docks to the kinase active site and forms hydrogen bonds with the protein through several ordered water molecules (Fig. 4*A*). The amidopropyl dimethylamino moiety contacts the hinge and the αD helix through hydrophobic interactions and solvent-mediated hydrogen bonds (Fig. 4 *C* and *D*). Its carbonyl group hydrogen bonds with an ordered water molecule that also hydrogen bonds to Asp293 (side chain, αD helix) and Ser290 (main chain). The dimethylamino group docks to a hydrophobic groove formed between the hinge and the αD helix. The benzimidazole and cyclobutane interact with the hinge, β1, β2, and β7 through van der Waals contacts. Unlike other ATP mimetic inhibitors of ALK2 (20), the benzimidazole does not hydrogen bond with the backbone amide of H284. Instead, its hydrogen bonds to an ordered solvent molecule that is hydrogen bonded to the backbone carbonyl of H284 and the backbone amide of H286. The cyclobutane interacts with Gly215 and Tyr219 of the gly-rich loop located above and Ser290 near the αD helix below (Fig. 4*C*). The 3,4,5-trimethoxyphenyl contacts the back pocket of the active site through hydrophobic interactions and solvent-mediated hydrogen bonds similarly to the ALK2 inhibitor K02288 (41). The 3-methoxy moiety hydrogen bonds to an ordered water that hydrogen bonds with the side chain of Lys235 (catalytic residue), and the 4-methoxy hydrogen bonds to another water that hydrogen bonds to both Lys235 and Glu248 (αC helix). Other high affinity ALK2 inhibitors with the trimethoxyphenyl moiety show similar water-mediated interactions with Lys235 but lack the interaction with Glu248 (41).

CDD-2281 and CDD-2282 show nearly identical interactions compared to CDD-2789, including the solvent-mediated interactions with the active site. They do not form any direct hydrogen bonding interaction with the active site (*SI Appendix*, Fig. S6 *A* and *B*).

The K_d values of compounds in *SI Appendix*, Table S1 are consistent with the crystal structures of ALK2:inhibitor complexes and provide further insights into their interaction. For

Table 1. Kinase selectivity data for compounds CDD-2342, CDD-2789, and LDN-193189

Kinases	CDD-2342 K_d (nM)	CDD-2789 K_d (nM)	LDN-193189 K_d (nM)
ACVR1 (ALK2)	1.64 ± 0.16	2.1 ± 0.2	0.04 ± 0.03
ACVRL1 (ALK1)	3.2 ± 0.7	3.9 ± 0.9	1.2 ± 0.13
BMPR1A (ALK3)	113 ± 24	541 ± 46	0.28 ± 0.05
ACVR1B* (ALK4)	N/A	N/A	64 ± 18
TGFBR1 (ALK5)	N/A	847 ± 46	3.3 ± 0.4
BMPR1B (ALK6)	301 ± 25	254 ± 19	0.13 ± 0.03
LCK*	N/A	71	N/D
SLK	N/A	N/D	N/D

N/A, not active at 1 μM concentration; N/D, not determined. *Z′-LYTE inhibition assays giving K_i values as described in *SI Appendix*.

example, removing all methoxyl moieties of R^3 (CDD-2317) weakens affinity significantly, suggesting that methoxyl moieties at all positions (CDD-2313, CDD-2420, CDD-2421) contribute to their high affinity. Substituting with fluorine (F) reduces molecule CDD-2340 affinity, suggesting that the water-mediated hydrogen bonds with the meta methoxyl moiety is also important. Substituting one of the methoxyl moieties with F while maintaining one other methoxyl (CDD-2617 and CDD-2618) does not significantly reduce molecule affinity since the pocket can accommodate a smaller F while the methoxyl maintains the solvent-meditated hydrogen bonds. Keeping one methoxy (CDD-2313) is enough to maintain high affinity (K_d = 5.6 nM). Replacing the methoxyphenyl with bulky functional groups reduces its affinity significantly since the back pocket near the αC-helix is shallow and bulky group likely clashes with the αC-helix. R^1 and R^2 makes little contact with the active site while pointing toward solvent consistent with the findings that replacement with various small or bulky functional groups at these positions does not affect its affinity since they will be exposed to solvent without forming any clash with the active site.

Compound CDD-2789 is ~400-fold selective for ALK1/2 over ALK4/5 (Table 1). The active site residues are highly conserved among ALKs, and the slightly larger gatekeeper residue for ALK1/2 (Thr) compared to ALK4/5 (Ser) means that simple steric exclusion by the gatekeeper can be ruled out as a basis for this selectivity. No structural information is available for ALK4, but comparisons with published ALK5 structures indicate that selectivity could arise from conformational differences that alter the relative positions of conserved active site residues between ALK5 and ALK2. Superimposing our ALK2:CDD-2789 structure and ALK5:ligand structure (PDB ID: 5USQ, 0.54 Å rmsd for 217 CA atoms) (42) reveals that the orientation of the αC-helix and its preceding loop differ between ALK2 and ALK5 (*SI Appendix*, Fig. S7). The difference in αC-helix tilt causes the aromatic ring of ALK2 Phe237 to protrude farther into the top of the active site than the corresponding Phe 234 of ALK5, while the side chain of ALK5 Tyr249 protrudes farther into the bottom of the active site than Tyr252 of ALK2. As a result, direct salt bridge formation occurs between Lys232:Glu245 in 5USQ but not between Lys235:Glu248 in our ALK2:CDD-2789 complex. Instead, in our structure, Lys235 and Glu248 hydrogen bond to a water that also hydrogen bonds to a CDD-2789 methoxy group. The Lys232 and Glu235 side chains hydrogen bond to another water; one water also hydrogen bonds to a second ligand methoxy group, while the other hydrogen bonds to Tyr252 side chain OH and to Asp354 backbone N. The 5USQ structure also has a water hydrogen bonded to Tyr249 and Glu245, but the difference inside chain positions mean that these two analogous waters are 2.9 Å apart in the superimposed structures. We speculate that the network of solvent-mediated ALK2:CDD-2789: interactions would not be possible in ALK5 due to the differences in αC-helix positioning, which may be driven by sequence changes away from the active

Table 2. NanoBret, Metabolic stability, and solubility of selected lead compounds

Compounds	ALK2 IC_{50} (μM)	ALK2 (R206H) IC_{50} (μM)	ALK1 IC_{50} (μM)	Assay (half-life)* MLM $t_{1/2}$ (min.)	Assay (half-life)* HLM $t_{1/2}$ (min.)	Solubility (μM)
LDN193189	0.040	0.057	1.775	–	–	–
CDD-2281	>30	>30	>30	807	769	199.6
CDD-2315	0.57	1.23	>30	6.3	7.8	63.5
CDD-2342	0.79	1.53	11.65	U	U	10.4
CDD-2340	5.30	9.25	>30	7.1	24.4	121.8
CDD-2421	1.24	2.40	>30	3.7	6.0	44.8
CDD-2469	4.72	4.45	>30	–	–	–
CDD-2617	10.70	13.40	>30	78.5	194	185.8
CDD-2787	0.47	0.71	>30	3.3	9.8	75.4
CDD-2789	0.54	1.13	10.07	505	2,767	200
CDD-2790	1.82	2.27	>30	6.1	9.0	153.8
CDD-2791	1.08	2.61	>30	2.8	15.4	128.1
CDD-2792	0.36	0.85	29.00	10	38.3	148.6
CDD-2793	2.72	4.28	>30	–	–	–
CDD-2794	2.09	3.16	>30	–	–	–
CDD-2795	0.39	0.46	8.55	2.9	17.0	141.5
Control	–	–	JQ1	12	14	–
			Alprazolam	258	620	–

*The half-life less than 30 min and clearance larger than 47.0 μL/min/mg protein in MLM and HLM were generally considered as unstable. U, extremely unstable.

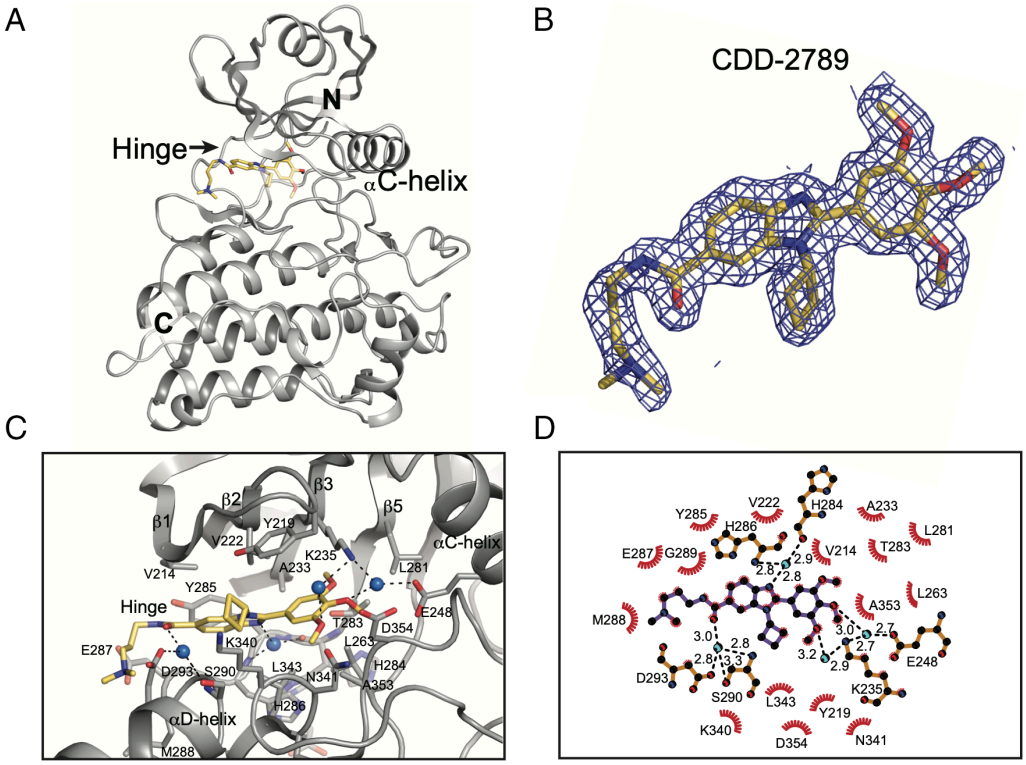

Fig. 4. Crystal structure of the ALK2/CDD-2789 complex. (*A*) Overall structure of the ALK2/CDD-2789 complex. Carbon atoms of CDD-2789 are in yellow, oxygens in red, and nitrogens in blue. Both termini are labeled. (*B*) 2*Fo-Fc* density for CDD-2789 contoured at 1σ. (*C*) Detailed interaction between ALK2 and CDD-2789. Key interacting residues shown are shown as sticks. Hydrogen bonds are shown with dashed lines. Water molecules that mediate hydrogen bonding interaction between ALK2 and CDD-2789 are shown in blue spheres. (*D*) LIGPLOT diagram (40) showing interactions between ALK2 and CDD-2789.

site, but which could also depend on the ligand. Differences in side-chain positions of ALK family lysine and glutamate residues and the water bridged network surrounding these residues has previously been invoked to explain ALK isotype selectivity (43).

NanoBRET™ (NB) Target Engagement (TE) Intracellular Kinase Analysis. To further evaluate ALK2 inhibitor activity and selectivity over ALK1 in cells, we performed NB TE intracellular kinase assays with WT ALK2, mutant ALK2 (R206H), and WT ALK1. Most of our potent inhibitors are more selective inhibitors against ALK2 and ALK2 (R206H) versus ALK1 (Fig. 5 and Table 2). CDD-2787 (cellular ALK2 IC_{50} = 0.47 μM), CDD-2789 (cellular ALK2 IC_{50} = 0.54 μM), CDD-2792 (cellular ALK2 IC_{50} = 0.36 μM), and CDD-2795 (cellular ALK2 IC_{50} = 0.39 μM) are the most potent and selective in our NB experiment (44, 45). To further access cellular kinome-wide selectivity of CDD-2789,

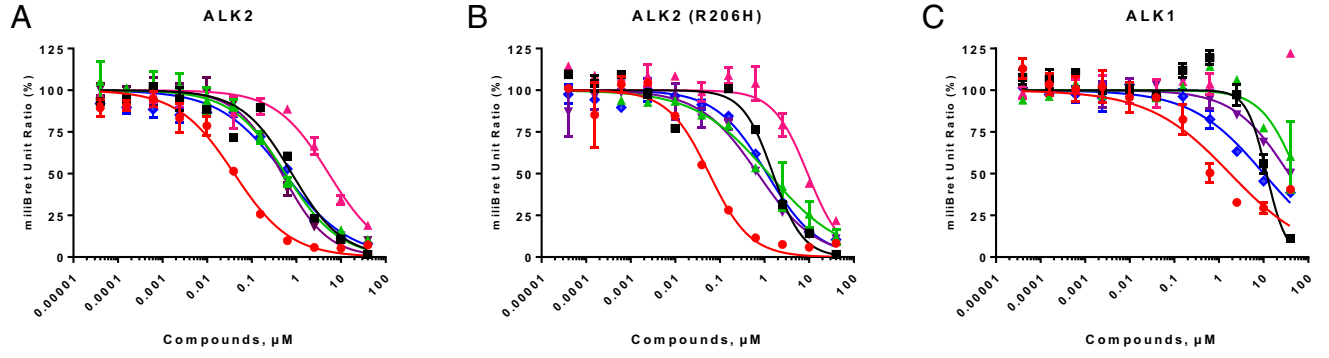

Compound	IC_{50} (μM) ALK2
LDN-193189	0.040
CDD-2315	0.57
CDD-2340	5.30
CDD-2342	0.79
CDD-2787	0.47
CDD-2789	0.54

Compound	IC_{50} (μM) ALK2(R206H)
LDN-193189	0.057
CDD-2315	1.23
CDD-2340	9.25
CDD-2342	1.53
CDD-2787	0.71
CDD-2789	1.13

Compound	IC_{50} (μM) ALK1
LDN-193189	1.775
CDD-2315	>30
CDD-2340	>30
CDD-2342	11.65
CDD-2787	>30
CDD-2789	10.07

Fig. 5. NB Assay of all key compounds. NB TE intracellular kinase assay performed with (*A*) WT ALK2, (*B*) mutant ALK2 (R206H), and (*C*) WT ALK1. LDN-193189 used as a control compound. IC_{50} shown in the μM.

we performed a NB K192 assay (Promega) at a high dose of 1 μM against 192 full-length protein kinases in HEK293 cells; TGFβ family receptor kinases are not included in the K192 assay. The results indicated that CDD-2789 is highly selective and does not engage with other kinases, with STK36 kinase being the closest with 20.22% occupancy (*SI Appendix,* Table S4).

Inhibition of BMP2-Induced Luciferase Activity in 293 T-BRE-Reporter Cells. We determined the cellular activities of the inhibitors using 293 T cells with a stably transfected BMP-responsive element driving the luciferase reporter (293 T-BRE-Luc) (2). 293 T-BRE-Luc cells with various concentrations of the ALK2 inhibitors CDD-2789, CDD-2315, and CDD-2787 (0.04, 0.2, 1, 5, or 25 μM) were pretreated for 30 min followed by the addition of 5 ng/mL of BMP2, 500 ng/mL BMP6, or 500 ng/mL BMP7 for 6 h. The impact of the inhibitors on luciferase transactivation was quantified and analyzed by calculating the change in luminescence relative to the ligand-treated samples. Relative to the vehicle-treated cells, BMP2, BMP6, and BMP7 treatments induced luciferase transactivation of the BRE reporter cells (Fig. 6 *A*, *C*, and *E*). Ligand-induced luciferase transactivation was decreased in a dose-dependent manner by addition of the CDD-2789, CDD-2315, and CDD-2787 inhibitors. The luminescence values were analyzed using a nonlinear regression model, which indicated that CDD-2789 had an IC_{50} of 2.14 μM, CDD-2315 had an IC_{50} of 1.49 μM and CDD-2787 had an IC_{50} of 0.94 μM under BMP2 stimulation (Fig. 6*B*). Similarly, under the BMP6 stimulation condition, CDD-2789 had an IC_{50} of 3.26 μM, CDD-2315 had an IC_{50} of 1.46 μM and CDD-2787 had an IC_{50} of 0.97 μM (Fig. 6*D*). In addition, CDD-2789 had an IC_{50} of 2.61 μM, CDD-2315 had an IC_{50} of 0.98 μM and CDD-2787 had an IC_{50} of 1.09 μM (Fig. 6*F*).

Inhibition of pSMAD1/5 in Primary WT and FOP Fibroblasts. More than 95% of patients with FOP harbor an activating mutation in ALK2 (R206H), leading to the development of ectopic bone formation (30). Inhibition of the mutant would be beneficial for patients, and we can test downstream signaling by inhibiting ALK2 as a surrogate for ALK2 (R206H). Therefore, we tested the ability of the ALK2 inhibitors to suppress activin A–induced phosphorylation of SMAD signaling in primary fibroblasts that were isolated from an individual with FOP (GM00513) (Fig. 7 *A* and *B*), as well as the BMP2-induced phosphorylation of SMAD1/5

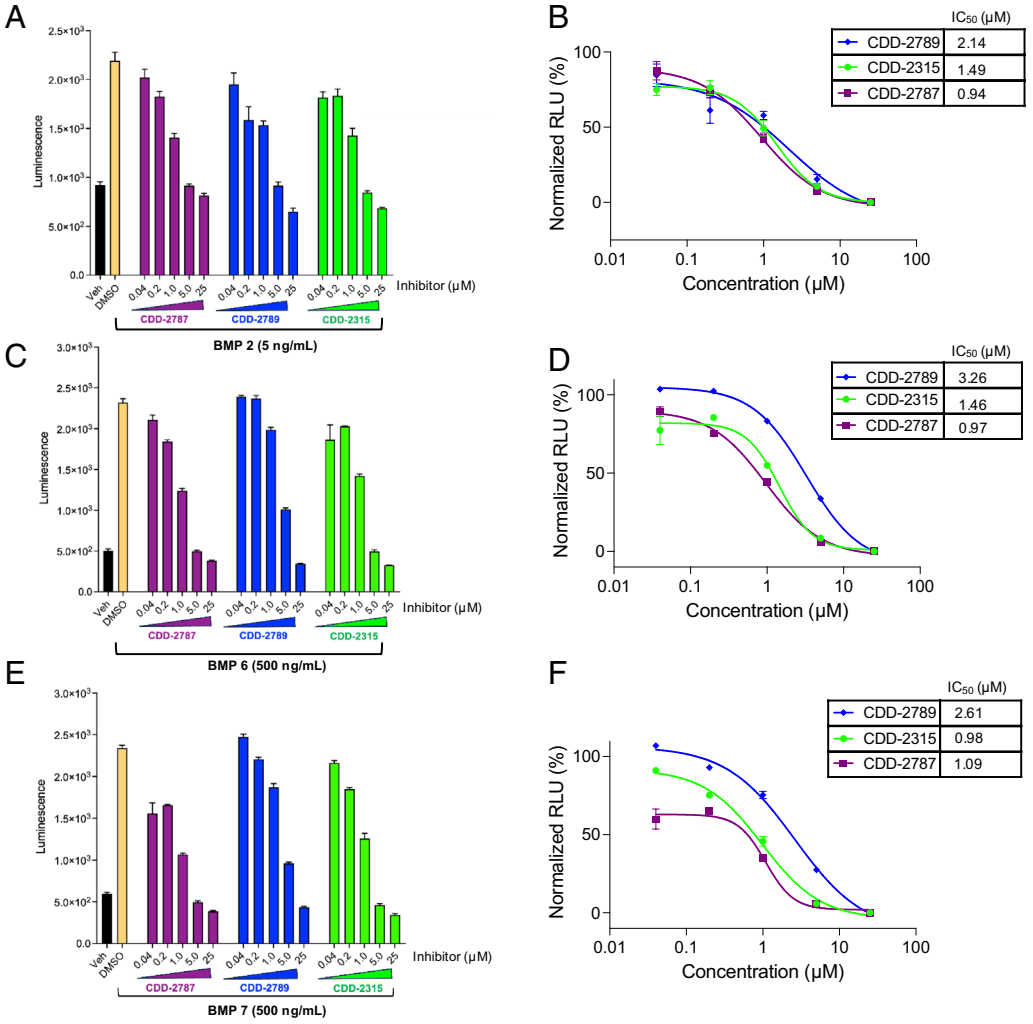

Fig. 6. Inhibition of BMP2, BMP6, and BMP7-induced luciferase activity in 293 T-BRE-reporter cells. Approximately 20,000 cells per well were plated in a 96-well plate and allowed to attach overnight. The following morning, cells were pre-treated with Vehicle dimethyl sulfoxide (DMSO) or ALK2 inhibitors, CDD-2789, CDD-2315, and CDD-2787 at various concentrations (0.04, 0.2, 1, 5, or 25 μM) for 30 min in phenol-red free Dulbecco's modified eagle medium (DMEM) supplemented with 2 mM Glutamine and 2% heat-inactivated FBS. Cells were then stimulated with vehicle or 5 ng/mL BMP2 (*A* and *B*), 500 ng/mL BMP6 (*C* and *D*), or 500 ng/mL BMP7 (*E* and *F*) for 6 h. Luciferase transactivation was assessed using the BrightGLO assay (Promega), and the emitted luminescence was quantified using a plate reader (M1000 Pro) and plotted as relative luminescence units (*A*, *C*, and *E*) or as a dose–response curve from the normalized relative luminescence units (RLU) (*B*, *D*, and *F*). IC_{50} was calculated using a nonlinear fit regression analysis of the normalized luminescence values and the equation, Y = Bottom + (Top-Bottom)/(1 + 10^((LogIC$_{50}$-X)*HillSlope)).

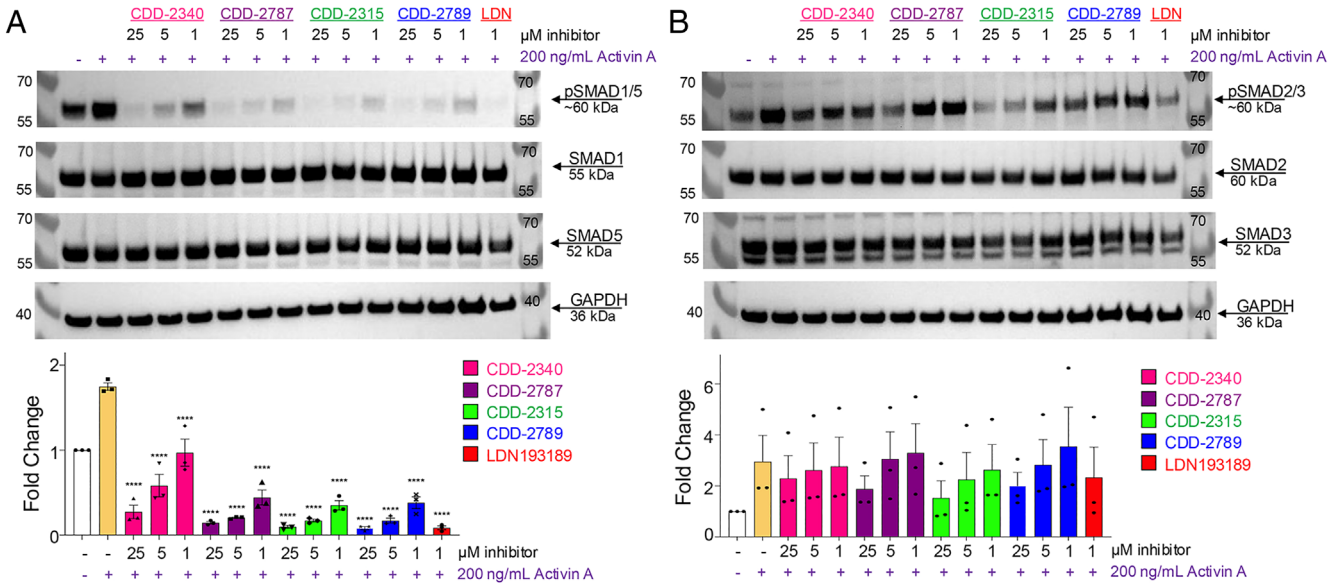

Fig. 7. Inhibition of pSMAD1/5 in primary FOP fibroblasts. (*A* and *B*) Primary fibroblasts isolated from a patient with fibrodysplasia ossificans progressiva (FOP GM00513) were pre-treated with various concentrations of ACVR1 inhibitors, CDD-2340, CDD-2787, CDD-2315, CDD-2789 (25, 5, or 1 μM), or LDN-192189 (1 μM) for 30 min. They were then treated with Vehicle (DMSO) or 200 ng/mL activin A in the presence of the inhibitors for 45 min. Cell lysates were then probed with antibodies against pSMAD1/5, total SMAD5, total SMAD1 and GAPDH (loading control) (*A*) or pSMAD2/3, total SMAD1, total SMAD5 and GAPDH (*B*) using a Western blot. Densitometric analyses of pSMAD1/5 or pSMAD2/3 were positioned below each Western Blot image respectively. (n = 3 biological replicates, one-way ANOVA with Tukey's post hoc analysis). Densitometric analyses of pSMAD1/5 or pSMAD2/3 are positioned below each western Blot image, respectively.

in primary fibroblasts that were isolated from an individual with FOP (GM00513) and a normal healthy individual (GM01652) (*SI Appendix*, Fig. S8). The fibroblasts were pretreated with 1, 5, or 25 μM of the ALK2 inhibitors, CDD-2340, CDD-2787, CDD-2315, and CDD-2789, or with 1 μM LDN193189 for 30 min followed by stimulation with 200 ng/mL activin A (Fig. 7 *A* and *B*) or 5 ng/mL of BMP2 (*SI Appendix*, Fig. S8 *A* and *B*) for 45 min. Cell lysates were probed with pSMAD1/5 and total SMAD1 and SMAD5 antibodies to detect the inhibitors' ability to suppress activin A or BMP2-stimulated pSMAD1/5 activation. In the FOP cells, CDD-2315, CDD-2789, CDD-2787, and CDD-2340 significantly inhibit the activin A-induced phosphorylation of SMAD1/5 starting at the 1 μM concentration (Fig. 7*A*). Interestingly, treatment of the aforementioned CDD compounds does not significantly affect the phosphorylation of SMAD2/3 induced by activin A (Fig. 7*B*). While CDD-2340 potently reduced BMP2-induced pSMAD1/5 activation in the WT fibroblasts at 5 and 25 μM (*SI Appendix*, Fig. S8*A*), only the highest concentration (25 μM) was sufficient to significantly reduce pSMAD1/5 activation in FOP cells (*SI Appendix*, Fig. S8*B*). CDD-2787 and CDD-2789 significantly reduced pSMAD1/5 activation in both cell types at all concentrations tested. CDD-2315 significantly reduced pSMAD1/5 at all the concentrations tested in WT fibroblasts (*SI Appendix*, Fig. S8*A*); however, the 1 μM dose of CDD-2315 did significantly reduce pSMAD1/5 activation by BMP2 in FOP cells (*SI Appendix*, Fig. S8*B*). The 1 μM dose of LDN193198 effectively suppressed pSMAD1/5 activation in both cell types and stimulation conditions (Fig. 7*A* and *SI Appendix*, Fig. S8).

In Vivo Efficacy in *ALK2*^{Q207D} Transgenic Mouse. To determine potential in vivo efficacy of our ALK2 inhibitor in the *ALK2*^{Q207D} transgenic mouse, HO (46) was induced in both legs of 12 mice (total 24 legs), and three males and three females were treated with 30 mg/kg of CDD-2789 while two males and four females received vehicle. Representative X-ray radiograms are shown in *SI Appendix*, Fig. S9. The Faxitron score from the CDD-2789 treated groups was 2.58 ± 0.90, while that from the vehicle controls was 1.75 ± 1.36 and no improvements were observed in either sex. The HO induction regime that we used does not cause any HO in wild type mice (47). Pilot studies at the doses of 20 mg/kg and 50 mg/kg gavaged once in a day also showed no reduction in HO formation compared to the vehicle controls. It is possible that not enough of the CDD-2789 may be reaching the site of HO formation, indicating that we may need to improve the pharmacokinetics of CDD-2789 analogs as a future direction.

Conclusions

ALK2 is a type 1 receptor for BMPs that transduces signals to the intracellular space by inducing the phosphorylation and activation of the SMAD1/5/8 transcription factors. ALK2 is one of seven type 1 ALK receptors (ALK1, ALK3, ALK4, ALK5, ALK6, and ALK7), and while key features are shared among them, they also have unique structural differences and tissue-specific expression patterns. The structural basis for activation of the type 1 receptors resides in the regulatory GS rich domain located in the intracellular region near the KD (48). In the absence of a ligand, FKBP12 binds atop the GS domain, blocking access to the type II receptor's phosphorylation potential (48). The ALK2 R206H mutation disrupts the inhibitory potential created by FKBP12 and the GS domain, rendering mild activation of the ALK2 receptor. Interestingly, in addition to transmitting unopposed signaling by the BMPs, the ALK2 mutation also becomes inappropriately activated by activin A, leading to downstream phosphorylation and activation of the SMAD1/5/8 transcription factors (49).

Activating mutations of the ALK2 receptor are prevalent in patients with FOP, who develop ectopic bone formation and experience premature lethality as a sequela to their disease (50). Activating ALK2 mutations have been identified in a subset of tumors from patients with DIPG (12, 51) and ependymomas (52). Endometrial tumors have also shown the presence of activating ALK2 mutations; however, the extent of their contribution to tumorigenesis is not well characterized (53, 54). Hence, there is a strong interest in developing small molecules that can inhibit

the kinase activity of the ALK2 receptors. Previous studies have identified ALK2 inhibitors showing efficacy against cell and animal models of FOP (9, 23, 55), DIPG (56), and iron deficiency anemia (57); however, specificity, stability, and toxicity are ongoing challenges (20).

To address this need, here we utilized DEC-Tec for the identification of small molecule inhibitors of ALK2. By performing an affinity selection with ALK2 using 3.94 billion DNA-barcoded molecules, we enriched for compounds having a benzimidazole core structure. Validation of these compounds by off-DNA synthesis and a minimal medicinal chemistry campaign rapidly led to the synthesis of the high-affinity ALK2 inhibitors CDD-2622, CDD-2206, CDD-2205, CDD-2341, and CDD-2342. CDD-2342 (MW: 611 Da) exhibits high selectivity for ALK2/ALK1 compared to over 408 other off-target kinases in KINOMEscan analysis but is metabolically unstable due to its high molecular weight. Subsequent SAR investigations resulted in the discovery of CDD-2789 (MW: 466 Da), which possesses greater potency, lower molecular weight, metabolic stability, high solubility, and higher selectivity for ALK2 over ALK1 in the NB cell-based assay.

KINOMEscan analysis revealed that CDD-2789 exhibits remarkable selectivity among a pool of over 408 off-target kinases, while confirmation of cellular selectivity was provided by the NB K192 assay (Promega). In vivo studies demonstrated a prolonged half-life and absence of toxicity for CDD-2789. Furthermore, we found that ALK2 inhibitors effectively reduced activin A or BMP2-induced pSMAD1/5 activation in fibroblasts from FOP individuals. We also tested the in vivo efficacy of CDD-2789 in a well-established $ALK2^{Q207D}$ transgenic mouse model that develops HO. The mice were gavaged once daily with 20 mg/kg and 50 mg/kg doses; however, we found no benefit in the reduction in the formation of HO compared to the vehicle controls. Pharmacokinetic studies of CDD-2789 showed that this compound has a plasma $t_{1/2}$ of 3.42 h, suggesting that increasing the frequency of compound administration may be necessary to observe an effect. Chemical probes are powerful tools within the therapeutic discovery process since they can evaluate whether a disease-ameliorating effect can be achieved through specific target modulation. Given the association of ALK2 within a variety of human disorders, CDD-2789, will serve as an invaluable tool for initiating the development of new agents in the clinic.

Materials and Methods

Methods and procedures for the synthesis of compounds, ALK2 KD protein expression and purification for crystallography, data collection, and structure solution, and analysis of small molecule activity in mammalian cell cultures are available in *SI Appendix*.

DNA-Encoded Chemical Library Affinity Selection with ALK2. DECL selection was performed as previously described (2) using recombinant human ALK2 intracellular KD protein (amino acid 147-end) that was purchased from Eurofins. Cheminformatic analyses of the sequencing data from the selections were performed using our informatics pipeline as described (31).

Calculation of K_d Values for Kinase Inhibitors That Bind to the ATP Pocket of a Kinase from LanthaScreen Binding Data. Dynafit (58) was used to fit complex equilibria where an ATP-competitive tracer is displaced by a dilution series of an ATP-competitive kinase inhibitor. This method relies on the concentration of inhibitor, as well as the concentration of kinase and tracer, and K_d of the tracer. The latter three parameters are tabulated by ThermoFisher for each kinase in the LanthaScreen assay panel.

Calculation of K_i Values for Kinase Inhibitors from Z′-LYTE Inhibition Data. The Morrison equation with [ATP] = K_m^{app} for competitive inhibition (GraphPad Prism7 software) was used to calculate K_i values. Since K_d and K_i values are defined the same way (K_d = [E] [I]/[EI] = K_i), K_d and K_i values can be compared.

NB TE Intracellular Kinase Assay. HEK293T cells were cultured in DMEM (Gibco11965-092) with 10% Fetal bovine serum (FBS) and 1% Pen-Strep (Gibco 15140-122) in 5% CO_2 incubator at 37 °C. HEK293T cell line underwent authentication by short tandem repeat profiling analysis. NB™ TE Intracellular Kinase Assay, K-11 (Cat. # N2651) transfection reagent FuGENE® HD (Cat. # E2311), transfection Carrier DNA (Cat. # E4881), ALK2-NanoLuc® Fusion Vector (Cat. # NV 2341, ALK2 (R206H)-NanoLuc® Fusion Vector (Cat. #, NV 2381) and ALK1-NanoLuc® Fusion Vectors (Cat. # NV 2391) were purchased from Promega. The measurement of test compounds TE was performed on 384-well format according to the manufacturer's (Promega) instructions.

HEK293 cells were transiently transfected with NanoLuc® ALK2, ALK2 (R206H), and ALK1 Fusion Vectors respectively. After 40 h of transfection, cells were treated with fixed conc of tracer followed by compounds (inhibitors) for 2 h of incubation. To determine the test compound affinity, cells were titrated with varying concentrations of compounds ranging from 40 μM to 0.4 nM at a fixed tracer concentration as recommended by Promega. LDN-193189 and Staurosporine were measured in parallel as a positive control. Freshly prepared NB Nano-Glo substrate plus extracellular NanoLuc inhibitor was added to initiate the subsequent bioluminescence resonance energy transfer (BRET) measurements using a CLARIOstar plus BMG LABTECH plate reader instrument. Data analysis was done by measuring the ratio of acceptor emission to donor emission (BRET ratio) and normalized by subtracting no-tracer-control background.

Additional ALK2/ALK1 Small Molecule Synthesis and Analyses. Synthesis of ALK2/ALK1 small molecule inhibitors and NMR, LCMS, and high resolution mass spectrometry analyses of the compounds were performed as described (2, 32). NB K192 assay, cytotoxicity assay, pharmacokinetics, dynamic solubility assay, and metabolic stability studies were performed as described (2, 32). Abbreviations presented in experimental procedures are defined as follows: HATU, O-(7-azabenzotriazol-1-yl)-N,N,N′,N′-tetramethyluronium hexafluorophosphate; DMF, N,N-dimethylformamide; NEt_3, triethylamine; EtOH: ethanol; DCM, dichloromethane; $Na_2S_2O_4$, sodium dithionite; EtOAc, ethyl acetate; Na_2SO_4, sodium sulfate.

Data, Materials, and Software Availability. Protein crystallography data have been deposited in PDB (9D8F (59), 9D8Z (60), 9D8E (61)). All other data are included in the article and/or *SI Appendix*.

ACKNOWLEDGMENTS. We thank Dr. Murugesan Palaniappan for help with selection experiments, Dr. Fei Yuan for assisting in bioinformatic analysis, and Dr. Mingxing Teng for his valuable discussions on the design of inhibitors. These studies were supported by the *Eunice Kennedy Shriver* National Institute of Child Health and Human Development grants R00-HD096057 (D.M.), R01-HD105800 (D.M.), and R01-HD032067 (M.M.M.). D.M. holds a Next Gen Pregnancy Award (NGP10125) from the Burroughs Wellcome Fund. The BCM Macromolecular X-ray Crystallography Core is funded in part by an NIH Shared Instrumentation Grant Award (S10OD030246). The ALS-ENABLE beamlines are partially supported by the NIH, National Institute of General Medical Sciences, grant P30 GM124169-01. The Advanced Light Source operates as a Department of Energy Office of Science User Facility under Contract No. DE-AC02-05CH11231.

Author affiliations: [a]Center for Drug Discovery, Baylor College of Medicine, Houston, TX 77030; [b]Department of Pathology & Immunology, Baylor College of Medicine, Houston, TX 77030; [c]Department of Molecular and Human Genetics, Baylor College of Medicine, Houston, TX 77030; [d]Department of Molecular and Cellular Biology, Baylor College of Medicine, Houston, TX 77030; [e]Department of Biologic and Materials Science, School of Dentistry, University of Michigan, Ann Arbor, MI 48109; [f]Promega Corporation, Madison, WI 53711; [g]Molecular Biophysics and Integrated Bioimaging, Berkeley Center for Structural Biology, Lawrence Berkeley National Laboratory, Berkeley, CA 94720; and [h]Verna and Marrs McLean Department of Biochemistry and Molecular Pharmacology, Baylor College of Medicine, Houston, TX 77030

Author contributions: R.J., D.M., Z.L., and M.M.M. designed research; R.J., D.M., H.M.T., K.L.S., K.M.B., Z.L., J.M.H., J.-Y.L., H.P., X.Q., B.S., Z.T., S.T., Y.M.V., and J.W. performed research; M.B.R. contributed new reagents/analytic tools; R.J., D.M., H.M.T., K.L.S., K.M.B., S.C., Z.L., F.L., J.-Y.L., Y.M., H.P., X.Q., M.B.R., B.S., Z.T., S.T., Y.M.V., J.W., D.W.Y., S.S.P., K.R.M., C.K., and M.M.M. analyzed data; M.M.M. conceptualization; and R.J., D.M., H.M.T., K.L.S., K.M.B., S.C., Z.L., F.L., Y.M., M.B.R., Z.T., J.W., D.W.Y., S.S.P., K.R.M., C.K., and M.M.M. wrote the paper.

1. T. Katagiri, T. Watabe, Bone morphogenetic proteins. *Cold Spring Harb. Perspect. Biol.* **8**, a021899 (2016).
2. R. K. Modukuri *et al.*, Discovery of highly potent and BMPR2-selective kinase inhibitors using DNA-encoded chemical library screening. *J. Med. Chem.* **66**, 2143–2160 (2023).
3. Y.-T. Xiao, L.-X. Xiang, J.-Z. Shao, Bone morphogenetic protein. *Biochem. Biophys. Res. Commun.* **362**, 550–553 (2007).
4. L. E. Gentry, B. W. Nash, The pro domain of pre-pro-transforming growth factor .beta.1 when independently expressed is a functional binding protein for the mature growth factor. *Biochemistry* **29**, 6851–6857 (1990).
5. A. M. Gray, A. J. Mason, Requirement for activin a and transforming growth factor–β1 pro-regions in homodimer assembly. *Science* **247**, 1328–1330 (1990).
6. J. L. Wrana, L. Attisano, R. Wieser, F. Ventura, J. Massagué, Mechanism of activation of the TGF-β receptor. *Nature* **370**, 341–347 (1994).
7. F. Liu *et al.*, A human Mad protein acting as a BMP-regulated transcriptional activator. *Nature* **381**, 620–623 (1996).
8. R. J. Pignolo, E. M. Shore, F. S. Kaplan, Fibrodysplasia ossificans progressiva: Diagnosis, management, and therapeutic horizons. *Pediatr. Endocrinol. Rev.* **10**, 437–448 (2013).
9. K. Sekimata, T. Sato, N. Sakai, ALK2: A therapeutic target for fibrodysplasia ossificans progressiva and diffuse intrinsic pontine glioma. *Chem. Pharm. Bull. (Tokyo)* **68**, 194–200 (2020).
10. C. Jones, L. Perryman, D. Hargrave, Paediatric and adult malignant glioma: Close relatives or distant cousins? *Nat. Rev. Clin. Oncol.* **9**, 400–413 (2012).
11. S. J. Dovedi *et al.*, Acquired resistance to fractionated radiotherapy can be overcome by concurrent PD-L1 blockade. *Cancer Res.* **74**, 5458–5468 (2014).
12. K. R. Taylor *et al.*, Recurrent activating ACVR1 mutations in diffuse intrinsic pontine glioma. *Nat. Genet.* **46**, 457–461 (2014).
13. F. S. Kaplan *et al.*, Dysregulation of the BMP-4 signaling pathway in fibrodysplasia ossificans progressiva. *Ann. N. Y. Acad. Sci.* **1068**, 54–65 (2006).
14. S. Ehata, K. Miyazono, Bone morphogenetic protein signaling in cancer; some topics in the recent 10 years. *Front. Cell Dev. Biol.* **10**, 883523 (2022).
15. D. Ye *et al.*, Insights into bone morphogenetic proteins in cardiovascular diseases. *Front. Pharmacol.* **14**, 1125642 (2023).
16. A. Duminuco *et al.*, ACVR1: A novel therapeutic target to treat anemia in myelofibrosis. *Cancers* **16**, 154 (2023).
17. C. Andersson-Rusch *et al.*, High concentrations of soluble endoglin can inhibit BMP9 signaling in non-endothelial cells. *Sci. Rep.* **13**, 6639 (2023).
18. J. Ma *et al.*, Inhibiting endothelial cell function in normal and tumor angiogenesis using BMP type I receptor macrocyclic kinase inhibitors. *Cancers* **13**, 2951 (2021).
19. H. Yin *et al.*, Inhibition of bone morphogenetic protein 6 receptors ameliorates Sjögren's syndrome in mice. *Sci. Rep.* **10**, 2967 (2020).
20. L. Rooney, C. Jones, Recent advances in ALK2 inhibitors. *ACS Omega* **6**, 20729–20734 (2021).
21. C. E. Sanvitale *et al.*, A new class of small molecule inhibitor of BMP signaling. *PLoS One* **8**, e62721 (2013).
22. H. Yamamoto *et al.*, Novel bicyclic pyrazoles as potent ALK2 (R206H) inhibitors for the treatment of fibrodysplasia ossificans progressiva. *Bioorg. Med. Chem. Lett.* **38**, 127858 (2021).
23. P. B. Yu *et al.*, Dorsomorphin inhibits BMP signals required for embryogenesis and iron metabolism. *Nat. Chem. Biol.* **4**, 33–41 (2008).
24. A. H. Mohedas *et al.*, Development of an ALK2-biased BMP type I receptor kinase inhibitor. *ACS Chem. Biol.* **8**, 1291–1302 (2013).
25. R. M. Franzini, D. Neri, J. Scheuermann, DNA-Encoded chemical libraries: Advancing beyond conventional small-molecule libraries. *Acc. Chem. Res.* **47**, 1247–1255 (2014).
26. Y. K. Sunkari, V. K. Siripuram, T.-L. Nguyen, M. Flajolet, High-power screening (HPS) empowered by DNA-encoded libraries. *Trends Pharmacol. Sci.* **43**, 4–15 (2022).
27. A. J. Davis *et al.*, An ALK2 inhibitor, BLU-782, prevents heterotopic ossification in a mouse model of fibrodysplasia ossificans progressiva. *Sci. Transl. Med.* **16**, eabp8334 (2024).
28. G. D. Cuny *et al.*, Structure-activity relationship study of bone morphogenetic protein (BMP) signaling inhibitors. *Bioorg. Med. Chem. Lett.* **18**, 4388–4392 (2008).
29. A. L. Satz *et al.*, DNA-encoded chemical libraries. *Nat. Rev. Methods Primer* **2**, 3 (2022).
30. A. Gironda-Martínez, E. J. Donckele, F. Samain, D. Neri, DNA-encoded chemical libraries: A comprehensive review with succesful stories and future challenges. *ACS Pharmacol. Transl. Sci.* **4**, 1265–1279 (2021).
31. J. C. Faver *et al.*, Quantitative comparison of enrichment from DNA-encoded chemical library selections. *ACS Comb. Sci.* **21**, 75–82 (2019).
32. A. F. Ku *et al.*, Reversible male contraception by targeted inhibition of serine/threonine kinase 33. *Science* **384**, 885–890 (2024).
33. C. Madasu *et al.*, Identification of potent pan-ephrin receptor kinase inhibitors using DNA-encoded chemistry technology. *Proc. Natl. Acad. Sci. U.S.A.* **121**, e2322934121 (2024).
34. R. K. Modukuri *et al.*, Discovery of potent BET bromodomain 1 stereoselective inhibitors using DNA-encoded chemical library selections. *Proc. Natl. Acad. Sci. U.S.A.* **119**, e2122506119 (2022).
35. Z. Yu *et al.*, Discovery and characterization of bromodomain 2–specific inhibitors of BRDT. *Proc. Natl. Acad. Sci. U.S.A.* **118**, e2021102118 (2021).
36. S. Dawadi *et al.*, Discovery of potent thrombin inhibitors from a protease-focused DNA-encoded chemical library. *Proc. Natl. Acad. Sci. U.S.A.* **117**, 16782–16789 (2020).
37. S. Chamakuri *et al.*, DNA-encoded chemistry technology yields expedient access to SARS-CoV-2 M^{pro} inhibitors. *Proc. Natl. Acad. Sci. U.S.A.* **118**, e2111172118 (2021).
38. R. Jimmidi *et al.*, DNA-encoded chemical libraries yield non-covalent and non-peptidic SARS-CoV-2 main protease inhibitors. *Commun. Chem.* **6**, 164 (2023).
39. S. Park *et al.*, Exploiting the carboxylate-binding pocket of β-lactamase enzymes using a focused DNA-encoded chemical library. *J. Med. Chem.* **67**, 620–642 (2024).
40. R. A. Laskowski, M. B. Swindells, LigPlot+: Multiple ligand-protein interaction diagrams for drug discovery. *J. Chem. Inf. Model.* **51**, 2778–2786 (2011).
41. A. H. Mohedas *et al.*, Structure-activity relationship of 3,5-diaryl-2-aminopyridine ALK2 inhibitors reveals unaltered binding affinity for fibrodysplasia ossificans progressiva causing mutants. *J. Med. Chem.* **57**, 7900–7915 (2014).
42. M. Sabat *et al.*, Design, synthesis and optimization of 7-substituted-pyrazolo[4,3-b]pyridine ALK5 (activin receptor-like kinase 5) inhibitors. *Bioorg. Med. Chem. Lett.* **27**, 1955–1961 (2017).
43. E. Williams, A. N. Bullock, Structural basis for the potent and selective binding of LDN-212854 to the BMP receptor kinase ALK2. *Bone* **109**, 251–258 (2018).
44. P. Puerto-Camacho *et al.*, Preclinical efficacy of endoglin-targeting antibody-drug conjugates for the treatment of ewing sarcoma. *Clin. Cancer Res.* **25**, 2228–2240 (2019).
45. N. Joubert, A. Beck, C. Dumontet, C. Denevault-Sabourin, Antibody-drug conjugates: The last decade. *Pharm. Basel Switz.* **13**, 245 (2020).
46. T. Fukuda *et al.*, Generation of a mouse with conditionally activated signaling through the BMP receptor, ALK2. *Genesis* **44**, 159–167 (2006).
47. H. Pan, N. Fleming, C. C. Hong, Y. Mishina, D. S. Perrien, Methods for the reliable induction of heterotopic ossification in the conditional Alk2Q207D mouse. *J. Musculoskelet. Neuronal Interact.* **20**, 149–159 (2020).
48. I. Quist-Løkken *et al.*, FKBP12 is a major regulator of ALK2 activity in multiple myeloma cells. *Cell Commun. Signal.* **21**, 25 (2023).
49. S. J. Hatsell *et al.*, ACVR1R206H receptor mutation causes fibrodysplasia ossificans progressiva by imparting responsiveness to activin A. *Sci. Transl. Med.* **7**, 303ra137 (2015).
50. E. M. Shore *et al.*, A recurrent mutation in the BMP type I receptor ACVR1 causes inherited and sporadic fibrodysplasia ossificans progressiva. *Nat. Genet.* **38**, 525–527 (2006).
51. K. R. Taylor, M. Vinci, A. N. Bullock, C. Jones, ACVR1 mutations in DIPG: Lessons learned from FOP. *Cancer Res.* **74**, 4565–4570 (2014).
52. D. Pratt *et al.*, Recurrent ACVR1 mutations in posterior fossa ependymoma. *Acta Neuropathol. (Berl.)* **144**, 373–376 (2022).
53. T. Fukuda, R. Fukuda, K. Miyazono, C.-H. Heldin, Tumor promoting effect of BMP signaling in endometrial cancer. *Int. J. Mol. Sci.* **22**, 7882 (2021).
54. J. A. Valer, C. Sánchez-de-Diego, C. Pimenta-Lopes, J. L. Rosa, F. Ventura, ACVR1 function in health and disease. *Cells* **8**, 1366 (2019).
55. J. Hao *et al.*, In vivo structure-activity relationship study of dorsomorphin analogues identifies selective VEGF and BMP inhibitors. *ACS Chem. Biol.* **5**, 245–253 (2010).
56. D. Carvalho *et al.*, ALK2 inhibitors display beneficial effects in preclinical models of ACVR1 mutant diffuse intrinsic pontine glioma. *Commun. Biol.* **2**, 156 (2019).
57. C. Mayeur *et al.*, Oral administration of a bone morphogenetic protein type I receptor inhibitor prevents the development of anemia of inflammation. *Haematologica* **100**, e68–e71 (2015).
58. P. Kuzmič, DynaFit–A software package for enzymology. *Methods Enzymol.* **467**, 247–280 (2009).
59. H. M. Ta, C. Kim, R. Jimmidi, M. M. Matzuk, Crystal structure of the ACVR1 (ALK2) Kinase Domain in complex with inhibitor CDD-2281. Protein Data Bank. https://www.rcsb.org/structure/unreleased/9D8F. Deposited 19 August 2024.
60. H. M. Ta, C. Kim, R. Jimmidi, M. M. Matzuk, Crystal structure of the ACVR1 (ALK2) Kinase Domain in complex with inhibitor CDD-2282. Protein Data Bank. https://www.rcsb.org/structure/unreleased/9D8Z. Deposited 20 August 2024.
61. H. M. Ta, C. Kim, R. Jimmidi, M. M. Matzuk, Crystal structure of the ACVR1 (ALK2) Kinase Domain in complex with inhibitor CDD-2789. Protein Data Bank. https://www.rcsb.org/structure/unreleased/9D8E. Deposited 19 August 2024.